

RESEARCH ARTICLE

A novel coordinated function of Myosin II with GOLPH3 controls centralspindlin localization during cytokinesis in *Drosophila*

Stefano Sechi^{1,*}, Anna Frappaolo^{1,*}, Angela Karimpour-Ghahnavieh¹, Roberta Fraschini² and Maria Grazia Giansanti^{1,‡}

ABSTRACT

In animal cell cytokinesis, interaction of non-muscle myosin II (NMII) with F-actin provides the dominant force for pinching the mother cell into two daughters. Here we demonstrate that *celibe* (*cbe*) is a missense allele of *zipper*, which encodes the *Drosophila* Myosin heavy chain. Mutation of *cbe* impairs binding of Zipper protein to the regulatory light chain Spaghetti squash (*Sqh*). In dividing spermatocytes from *cbe* males, *Sqh* fails to concentrate at the equatorial cortex, resulting in thin actomyosin rings that are unable to constrict. We show that *cbe* mutation impairs localization of the phosphatidylinositol 4-phosphate [PI(4)P]-binding protein Golgi phosphoprotein 3 (GOLPH3, also known as Sauron) and maintenance of centralspindlin at the cell equator of telophase cells. Our results further demonstrate that GOLPH3 protein associates with *Sqh* and directly binds the centralspindlin subunit Pavarotti. We propose that during cytokinesis, the reciprocal dependence between Myosin and PI(4)P–GOLPH3 regulates centralspindlin stabilization at the invaginating plasma membrane and contractile ring assembly.

KEY WORDS: *Drosophila*, Male meiosis, Cytokinesis, Myosin, GOLPH3

INTRODUCTION

Animal cell cytokinesis is accomplished by constriction of the contractile ring at the equatorial cortex (D'Avino et al., 2015). After anaphase onset, a structure composed by non-muscle myosin II (NMII) and filamentous actin (F-actin) is assembled just beneath the plasma membrane, providing the dominant force for pinching the dividing cell into two daughter cells. Three different genes in mammalian cells encode the NMII heavy chain (NMHC II) proteins, whereas only one gene encodes the *Drosophila* NMHC II protein Zipper (*Zip*) (Ketchum et al., 1990; Kiehart et al., 1989; Mansfield et al., 1996; Young et al., 1993).

The NMII molecule is a hexamer composed of two identical heavy chains, a pair of essential light chains (ELC) and a pair of regulatory light chains (RLC; Shutova and Svitkina, 2018; Fig. 1A). Each heavy chain contains a conserved N-terminal globular head domain with ATPase and actin-binding activity. One RLC and one ELC associate with each NMHC II via two IQ motifs on a neck region that connects

the head and tail domains (Fig. 1A). The NMHC II C-terminus has a long coiled-coil tail domain responsible for the assembly of NMII monomers into bipolar filaments (Murakami et al., 2000; Ronen and Ravid, 2009; Shutova and Svitkina, 2018; Vicente-Manzanares et al., 2009). Studies in multiple model systems demonstrated the essential role of NMHC II in normal cytokinesis (De Lozanne and Spudich, 1987; Echard et al., 2004; Eggert et al., 2004; Hickson et al., 2006; Ma et al., 2012; Mabuchi and Okuno, 1977; Osório et al., 2019; Straight et al., 2003, 2005; Wang et al., 2019). Analysis of myosin truncations revealed that targeting NMHC II to the cleavage furrow does not require the motor domain but involves signals in the tail (Beach and Egelhoff, 2009; Uehara et al., 2010). Total reflection fluorescence imaging of the cortex of dividing *Drosophila* S2 cells showed that NMII filaments are highly dynamic, suddenly concentrating at the equatorial cortex and disappearing from the poles (Vale et al., 2009). According to the most widely accepted model for NMII recruitment, *de novo* filament assembly occurs at the equatorial cortex via localized RLC phosphorylation, stimulated by the Rho pathway. During late anaphase, the small GTPase RhoA (Rho1 in *Drosophila*) stimulates F-actin filament formation in the cortex and controls contractile ring constriction by activating Rho kinase, which phosphorylates RLC on Thr-18 and Ser-19 (Eda et al., 2001; Ishizaki et al., 1996; Matsumura et al., 2011; Yamashiro et al., 2003). The evolutionarily conserved two protein complex centralspindlin, composed of two molecules of the kinesin family member MKLP1 [also known as KIF23 in humans; Pavarotti (Pav) in *Drosophila*] and two molecules of the Rho family GTPase-activating protein (GAP) CYK4 (also known as RACGAP1 in humans; RacGAP50C, encoded by *tumbleweed*, in *Drosophila*), has a key role in specifying the site of the cleavage furrow (D'Avino et al., 2006, 2015; Giansanti and Fuller, 2012). The balance between the active state (GTP-bound) and inactive state (GDP-bound) of RhoA/Rho1 requires the recruitment of the Rho guanine-nucleotide-exchange factor (GEF) ECT2 (Pebble in *Drosophila*) to the equatorial cortex, which is mediated by centralspindlin (Kamijo et al., 2006; Nishimura and Yonemura, 2006; Piekny et al., 2005; Somers and Saint, 2003; Yüce et al., 2005; Zhao and Fang, 2005).

Recent work suggests that the interaction with plasma membrane lipids might have an important role in localizing centralspindlin as well as NMII at the cleavage furrow (Basant et al., 2015; Lekontsev et al., 2012; Liu et al., 2016). The centralspindlin subunit CYK4 binds to phosphatidylinositol 4-phosphate [PI(4)P] and phosphatidylinositol 4,5-bisphosphate [PI(4,5)P₂] phosphoinositides at the furrow plasma membrane via its C1 domain (Lekontsev et al., 2012). Mammalian NMIIA, NMIIB and NMIIIC bind to negatively charged liposomes containing one or more acidic phospholipids, and NMIIA associates with plasma membrane of HeLa cells and fibrosarcoma when actin filaments are depolymerized (Liu et al., 2016). Moreover RLC interacts with PI(4)P and mediates plasma membrane localization of PI(4)P in dividing neuroblasts (Koe et al., 2018). In this context, we

¹Istituto di Biologia e Patologia Molecolari del CNR, Dipartimento di Biologia e Biotecnologie, Università Sapienza di Roma, Piazzale A. Moro 5, 00185 Roma, Italy.
²Dipartimento di Biotecnologie e Bioscienze, Università degli Studi di Milano Bicocca, 20126, Milano, Italy.

*These authors contributed equally to this work

‡Author for correspondence (mariagrazia.giansanti@uniroma1.it)

 M.G.G., 0000-0002-6753-7262

Handling Editor: David Glover

Received 13 August 2020; Accepted 7 October 2020

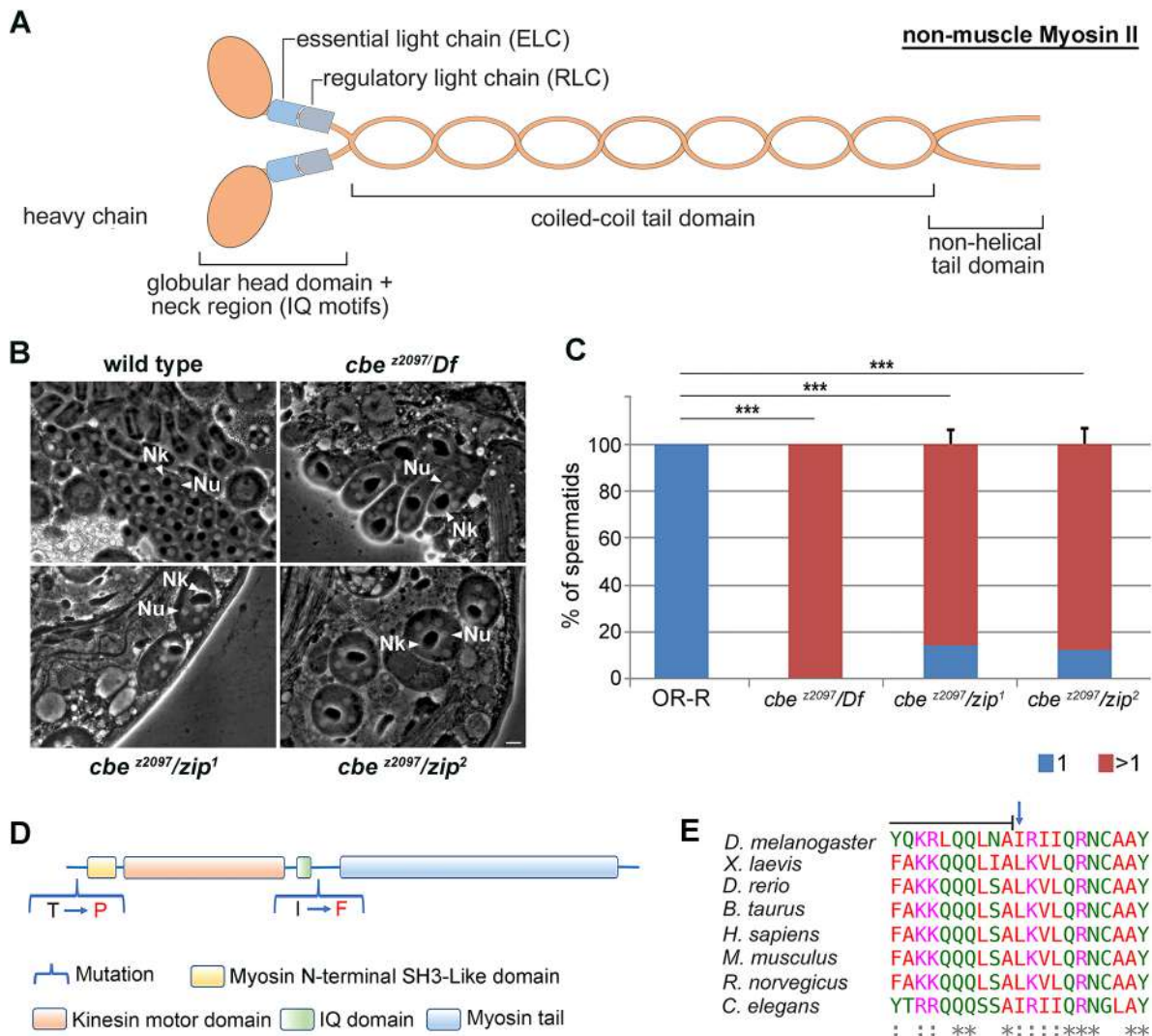


Fig. 1. *cbe* is a missense allele of the *zip* gene. (A) Schematic depicting the subunits and domain structure of non-muscle Myosin II. (B) Multinucleate onion stage spermatids due to cytokinesis failure during meiosis in *cbe^{z2097}* mutant males. Nu, nucleus; Nk, nebenkern (mitochondrial derivative). Scale bar: 10 μ m. (C) Frequencies of spermatids containing one or more than one nucleus per Nk, in control Oregon-R males (OR-R) and *cbe^{z2097}* mutant males. Graph shows mean \pm s.d. percentage. Spermatids were examined from testes of at least ten males per genotype. *** $P < 0.0001$ (Fisher's exact test). (D) Schematic showing the domain organization of Zip protein and the amino acids mutated in *cbe^{z2097}*. Permissive replacement of threonine (T) by proline (P), which is also present in the background chromosome, and substitution of phenylalanine (F) for wild-type isoleucine (I), which underlies the *cbe* phenotype, are indicated. (E) Alignment of a portion of *Drosophila* Zip protein with NMHC II proteins from different species. (*) fully conserved residue; (:) conservation between groups of strongly similar properties. Arrow points to the amino acid mutated in *cbe*. Line indicates the C-terminal end of the IQ motif (as determined using ScanProsite).

previously demonstrated that the PI(4)P-binding protein GOLPH3 (also known as Sauron) is required to stabilize NMII rings and to maintain centralspindlin at the cell equator of dividing cells in *Drosophila melanogaster* (Sechi et al., 2014).

Here, we show that *celibe* (*cbe*), identified during a screen for mutants affecting spermatocyte cytokinesis (Giansanti et al., 2004), is a missense allele of *Drosophila zipper* that affects contractile ring structure in both mitotic and meiotic cells. In *cbe* mutants, Zip protein is unable to bind the RLC protein Spaghetti squash (Sqh). *cbe* mutant spermatocytes display initial localization of Zip and Septin proteins at the cleavage site during late anaphase and early telophase but do not concentrate Sqh at the equatorial cortex. However, the contractile rings assembled in *cbe* mutant spermatocytes appear thin, fail to constrict and fragment during later stages of cytokinesis. We further show that *cbe* mutation impairs localization of GOLPH3 and maintenance of centralspindlin at the cleavage furrow. We demonstrate that GOLPH3

protein associates with Sqh and directly binds the centralspindlin subunit Pav. We propose that during cytokinesis, the reciprocal dependence between NMII and PI(4)P-GOLPH3 regulates centralspindlin stabilization and contractile ring structure at the cleavage site.

RESULTS

Molecular cloning of the *Drosophila celibe* gene

The *celibe^{z2097}* (*cbe^{z2097}*) allele was previously identified during a cytological screen for mutants affecting cytokinesis in *Drosophila* spermatocytes (Giansanti et al., 2004). *cbe^{z2097}* mutant males display multinucleate spermatids, indicating defective meiotic cytokinesis (Giansanti et al., 2004). Complementation analysis with a series of chromosomal deletions uncovering the second chromosome revealed that *cbe^{z2097}* complemented *Df(2R)BSC604* but failed to complement *Df(2R)BSC608* for both male sterility and the cytokinesis defects

(Fig. 1B), indicating that it maps to a genomic interval that contains the *zipper* (*zip*) gene, encoding the *Drosophila* non-muscle Myosin II heavy chain (Mansfield et al., 1996). The *zip* EMS-induced alleles *zip*¹ (Young et al., 1993; Zhao et al., 1988) and *zip*² (Young et al., 1993; Zhao et al., 1988) failed to complement *cbe*^{z2097} for male sterility and male meiotic failures, indicating that *cbe*^{z2097} is a mutant allele of *zip* (Fig. 1C,D). DNA sequencing of the *cbe*^{z2097} allele revealed two point mutations, relative to the reference sequence on FlyBase, in the *zip* gene (Fig. 1E). The first mutation is located in a 45-residue N-terminal extension of the Zip polypeptide (Mansfield et al., 1996), which is shared by three Zip isoforms (Flybase.org), resulting in the replacement of a threonine residue by proline (Fig. 1D). The second mutation is located within a highly conserved region common to all the Zip isoforms, resulting in the replacement of a conserved isoleucine by phenylalanine (Fig. 1D). However, the threonine-to-proline substitution is not likely to be the cause of the mutant phenotype, because the same substitution is also present prior to mutagenesis in the original fly line, which does not exhibit sterility and spermatocyte cytokinesis failures (Zuker line; Koundakjian et al., 2004). The conserved isoleucine is adjacent to the IQ motif, which is required for binding of Zip protein to the RLC Spaghetti squash (Sqh) (Fig. 1D,E; Trybus et al., 1994; Uehara et al., 2010). Western blot analysis of adult testis and larval brain extracts from *cbe*^{z2097}/*Df*(2R)*BSC608* (*cbe/Df*) mutants revealed reduced Zip protein levels, suggesting that that *cbe* mutation also affects the stability of Zip protein (Fig. S1A,B).

Contractile rings of *cbe* mutants fail to constrict

To gain further insight into the cytokinesis phenotype of the *cbe/Df* mutants, dividing spermatocytes were stained for Zip protein (Fig. 2A). All the spermatocytes from both wild-type and *cbe/Df* mutant males assembled Zip rings at the equatorial cortex during late anaphase and early telophase (Fig. 2A). However, in *cbe/Df* spermatocytes, localization of Zip protein at the cell equator was greatly reduced and associated with thin rings. Strikingly, in dividing spermatocytes from *cbe/Df* males the majority of Zip protein accumulated into cytoplasmic aggregates (Fig. 2A). Analysis of mid-to-late telophase revealed that 100% of wild-type spermatocytes displayed tight and constricted Zip rings (Fig. 2A). Conversely, in *cbe/Df* mutant spermatocytes, fixed at mid-telophase, Zip protein formed unconstricted and fragmented rings and was enriched in large cytoplasmic aggregates (Fig. 2A). Immunofluorescence analysis revealed that the RLC fused to green fluorescent protein, Spaghetti squash-GFP (Sqh-GFP; Royou et al., 2002) concentrated into an equatorial ring that colocalized with the Zip protein in wild-type telophase spermatocytes (Fig. 2B) but failed to accumulate in the cleavage furrow of *cbe/Df* telophases (Fig. 2B). Previous analyses failed to detect F-actin rings in *cbe* mutant spermatocytes (Giansanti et al., 2004). However, examination of fixed mutant spermatocytes using our improved F-actin staining protocol (Frappaolo et al., 2017a), revealed that *cbe/Df* mutant spermatocytes assembled F-actin rings that were substantially thinner than those in wild type and that failed to constrict (Fig. S2). Localization of Septins was also affected

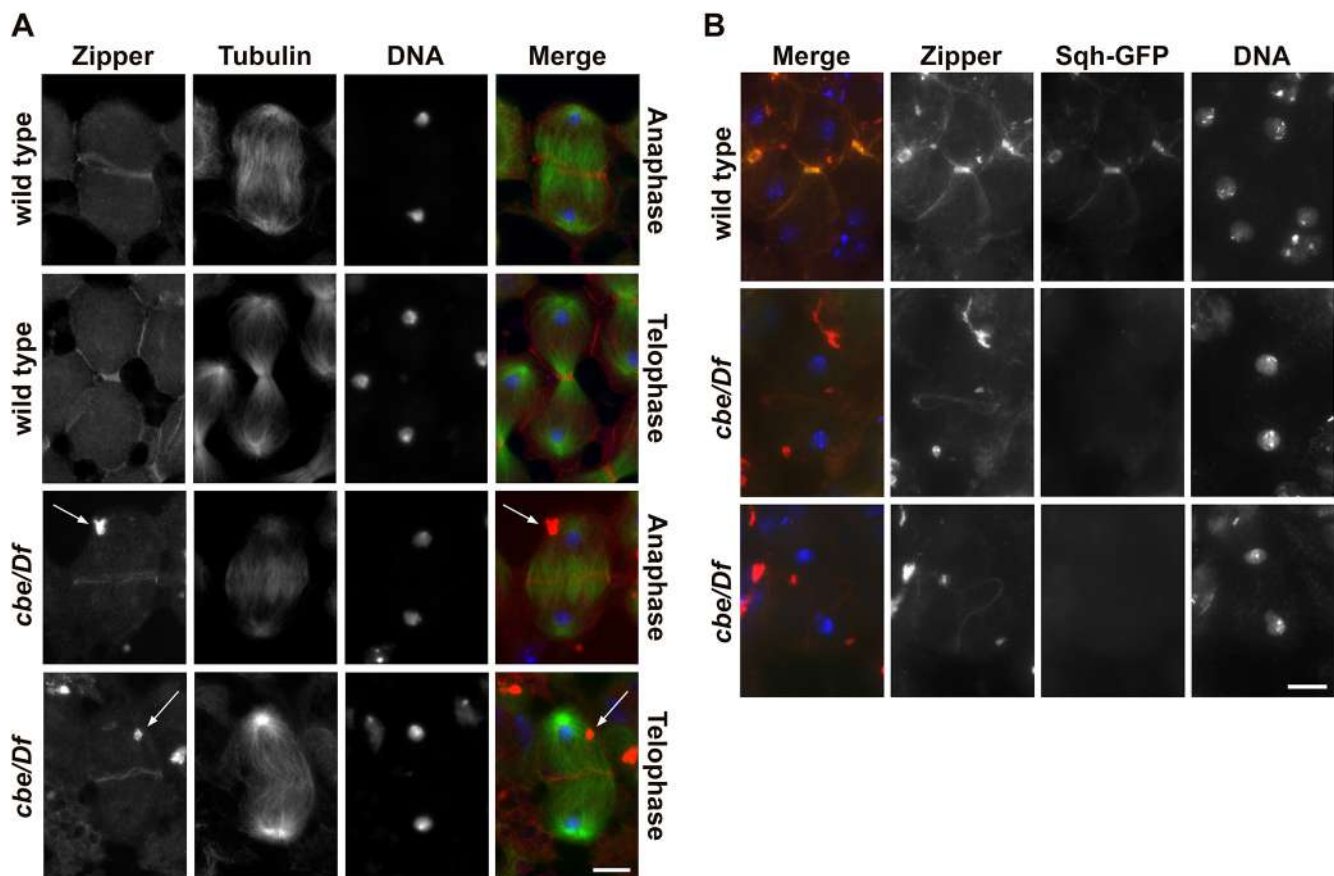


Fig. 2. The *cbe* mutation affects NMII distribution at the cleavage site. (A) Wild-type and *cbe*^{z2097}/*Df*(2R)*BSC608* (*cbe/Df*) mutant spermatocytes during late anaphase and mid-to-late telophase, stained for tubulin (green), DNA (blue) and Zip (red). *n*=40 wild-type and *cbe/Df* late-anaphase spermatocytes; *n*=60 wild-type and *cbe/Df* mid-to-late telophase spermatocytes; randomly selected from images taken in five experiments. Arrows point to cytoplasmic aggregates containing Zip protein. (B) Wild-type and *cbe/Df* mutant spermatocytes during late telophase, stained for Sqh (Sqh-GFP, green), DNA (blue) and Zip (red). *n*=40 wild-type and *cbe/Df* late telophase spermatocytes, randomly selected from images taken in five experiments. Scale bars: 10 μ m.

in *cbe* mutants. In wild-type and *cbe/Df* mutant spermatocytes at early telophase, the septin *Sept1* accumulated in the cleavage furrow (Fig. S3). However, Septin rings failed to constrict and fragmented in mid-to-late telophases of *cbe/Df* mutants (Fig. S3).

Wild-type function of Zip protein is required for cytokinesis in larval brain neuroblasts

Immunofluorescence analysis revealed that wild-type function of Zip was also required for normal contractile ring constriction in larval brain neuroblasts. In wild-type dividing neuroblasts stained for tubulin and Zip, Zip protein localized to the basal cortex during early anaphase and concentrated at the furrow during early telophase

(Fig. 3A). Immunostaining of *cbe/Df* mutant dividing neuroblasts revealed that Zip cortical localization was less robust than in wild type during both anaphase and telophase (Fig. 3B). Moreover *cbe/Df* mutant neuroblasts at late telophase failed to pinch the central spindle midzone during cytokinesis (Fig. 3A,B). Immunostaining of larval brains for tubulin and the contractile ring protein Anillin (Goldbach et al., 2010; Oegema et al., 2000) also revealed cytokinesis defects. Anillin accumulated at the cleavage furrow of both wild-type and *cbe/Df* mutant neuroblasts during telophase (Fig. 3C,D). However, in 70% of *cbe/Df* mutant neuroblasts at late telophase, the Anillin rings appeared large and unconstricted, a phenotype not observed in control neuroblasts (Fig. 3C,D).

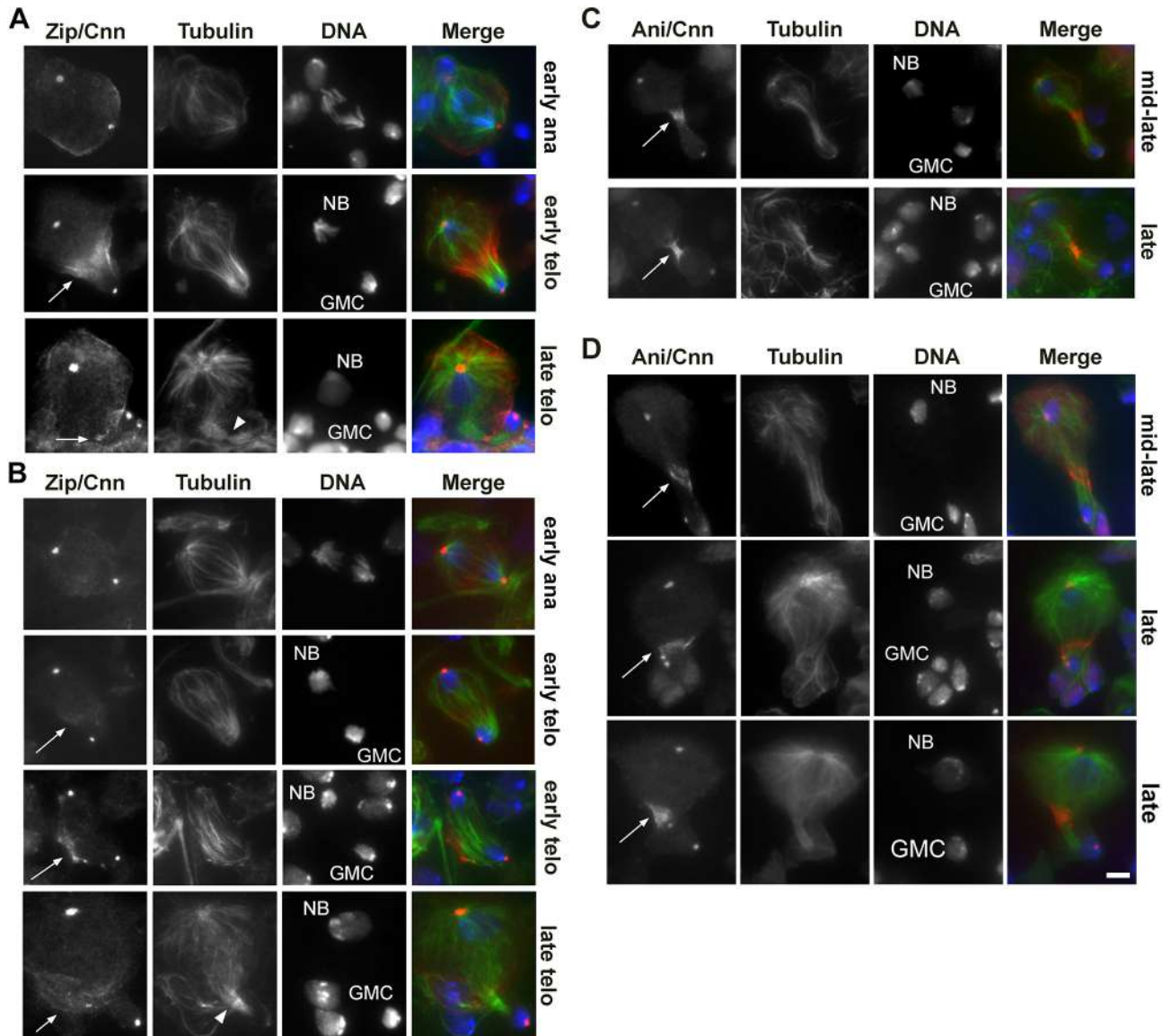


Fig. 3. Dividing neuroblasts from *cbe* mutants display defective contractile rings. (A,B) Wild-type (A) and *cbe²²⁰⁹⁷/Df(2R)BSC608* (*cbe/Df*) mutant (B) neuroblasts during early anaphase, early telophase and late telophase, stained for tubulin (green), DNA (blue) and Zip (red). Centrosomin staining (Cnn) is also shown (red). $n=25$ wild-type and *cbe/Df* early anaphase neuroblasts; $n=30$ wild-type and *cbe/Df* early telophase neuroblasts; $n=50$ wild-type and *cbe/Df* late telophase neuroblasts; randomly selected from images taken in five experiments. Arrows point to Zip accumulation, arrowheads point to the central spindle midzone. Note that the spindle midzone is pinched in the middle in wild-type late telophase but not in *cbe/Df* mutant late telophase. (C,D) Wild-type (C) and *cbe/Df* mutant (D) neuroblasts during telophase, stained for tubulin (green), DNA (blue) and Anillin (Ani; red). Centrosomin staining (Cnn) is also shown (red). $n=50$ wild-type and *cbe/Df* mid-to-late telophase neuroblasts; $n=40$ wild-type and *cbe/Df* late telophase neuroblasts; randomly selected from images taken in seven experiments. Arrows point to Anillin in constricted (wild type) and unconstricted (*cbe/Df*) rings. NB, neuroblast nucleus; GMC, ganglion mother cell nucleus. Scale bar: 5 μ m.

***cbe/Df* mutant spermatocytes display defective GOLPH3 and centralspindlin localization at the cleavage site**

We previously demonstrated that GOLPH3 protein accumulates at the cleavage furrow and is required for maintenance of NMII rings during cytokinesis (Sechi et al., 2014). Localization of GOLPH3 was abolished by *cbe* mutation. In wild-type dividing spermatocytes, GOLPH3 protein accumulated at the equatorial site during telophase (Fig. 4). In contrast, GOLPH3 protein was not detected at the cleavage site of *cbe/Df* mutant telophases (Fig. 4). Dividing spermatocytes from *cbe/Df* mutants also displayed defective central spindle structures (Figs 2, 4, 5; Fig. S3). Our previous work showed that GOLPH3 function enables maintenance of the centralspindlin complex at the cell equator during cytokinesis (Sechi et al., 2014). In agreement with these data, localization of the RacGAP50C component of the centralspindlin complex (D'Avino et al., 2006) was affected in *cbe/Df* mutant dividing spermatocytes during telophase (Fig. 5A–D). In wild-type and *cbe/Df* mutant spermatocytes stained for tubulin and RacGAP50C, RacGAP50C started to accumulate at the peripheral and interior microtubules during mid-anaphase (Fig. 5A,B). In early telophase spermatocytes from wild type, RacGAP50C formed a tight equatorial band at the midzone of the central spindle, which constricted during mid- and late telophase (Fig. 5A). Conversely, early telophase spermatocytes from *cbe/Df* mutants displayed a faint localization of RacGAP50C at the interior and the peripheral microtubules (Fig. 5A). During later stages of *cbe/Df* mutant telophase, RacGAP50C either failed to accumulate, or was enriched at the interior microtubules with no appreciable concentration at the cortex (Fig. 5A).

Anillin is thought to act as molecular scaffold that links the plasma membrane with the contractile ring (D'Avino, 2009; Kechad et al., 2012; Liu et al., 2012; Takeda et al., 2013). Moreover, previous studies in *Drosophila* demonstrated that RacGAP50C interacts directly with Anillin and provides a link between the actomyosin ring and the peripheral microtubules (D'Avino et al., 2008; Gregory et al., 2008). We thus immunostained dividing *cbe/Df* spermatocytes for either tubulin and Anillin (Fig. S4) or Anillin and RacGAP50C (Fig. 5C,D). In dividing wild-type and *cbe/Df* spermatocytes stained for tubulin and Anillin, Anillin started to accumulate at the cell equator during early anaphase and formed a circumferential band at the equatorial cortex during early telophase (Fig. S4). Consistent with previous observations of *cbe* homozygous mutants (Giansanti et al.,

2004), and unlike wild-type spermatocytes, *cbe/Df* spermatocytes stained at later stages of telophase displayed unconstricted Anillin rings (Fig. S4). In wild-type dividing spermatocytes stained for Anillin and RacGAP50C during mid-to-late telophase, the RacGAP50C equatorial band was juxtaposed with the Anillin ring (Fig. 5C,D). Conversely in mid-telophase spermatocytes from *cbe/Df* males, the Anillin ring and the spindle-associated RacGAP50C appeared dissociated (Fig. 5C,D).

***cbe* mutation affects Zip–Sqh interaction in *Drosophila* testis extracts**

Because the *cbe* mutation replaces a conserved isoleucine that is adjacent to the IQ motif (Fig. 1D,E), we asked whether the *cbe^{z2097}* mutant allele could influence the assembly of the Zip–Sqh complex. Co-immunoprecipitation (co-IP) analysis from testis extracts indicated that *cbe* mutation impaired the interaction of Zip protein with Sqh (Fig. 6A). Our previous findings suggested that GOLPH3 interacts with Zip and other cytokinesis proteins in *Drosophila* (Sechi et al., 2014). Moreover, recent work showed that Sqh protein binds to PI(4)P *in vitro* and mediates plasma membrane localization of PI(4)P in *Drosophila* neural stem cells (Koe et al., 2018). We then assessed whether GOLPH3 protein interacts with Sqh–GFP (Fig. 6A,B; Fig. S5). GST pull-down experiments showed that Sqh–GFP interacts with GOLPH3 (Fig. 6B). Co-IP experiments from adult testes indicated that GOLPH3 co-precipitated with Sqh–GFP (Fig. S5) and that the interaction partially depended on the Sqh–Zip complex (Fig. 6A).

Our previous work suggested that GOLPH3 associates with Pavarotti (Pav; Adams et al., 1998), the kinesin-like protein that works together with RacGAP50C in the centralspindlin complex (Sechi et al., 2014). Mislocalization of RacGAP50C at the cleavage site of *cbe* mutants led us to further investigate the GOLPH3–Pav interaction. Pav–YFP (Szafer-Glusman et al., 2008) was immunoprecipitated using antibodies against YFP and probed for GOLPH3 (Fig. 7A). To assess whether GOLPH3 could directly bind to Pav protein, we purified various Pav fragments (Bassi et al., 2013) tagged with glutathione S-transferase (GST) from bacteria and tested their ability to pull down 6×His–GOLPH3 (Fig. 7B–D). These experiments suggested that GOLPH3 interacts with the Pav stalk and tail C-terminal domains (Fig. 7C,D). These data were confirmed using yeast two-hybrid assays (Fig. 7E).

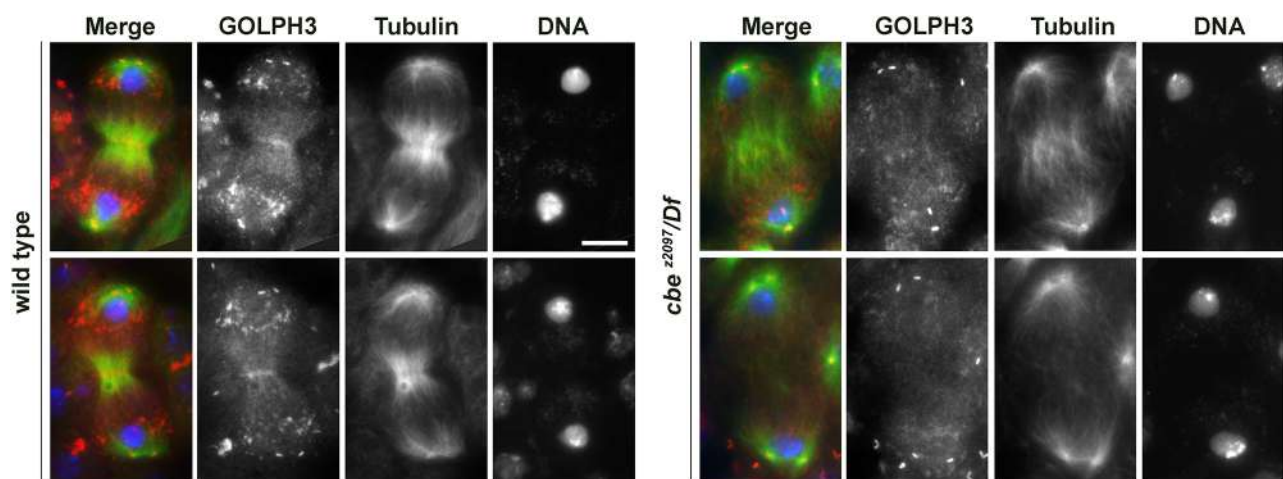


Fig. 4. The *cbe* mutation impairs GOLPH3 accumulation in the cleavage furrow of dividing spermatocytes. Wild-type and *cbe^{z2097/Df(2R)BSC608}* (*cbe^{z2097/Df}*) mutant spermatocytes during early telophase (top) and mid-to-late telophase (bottom), stained for tubulin (green), DNA (blue) and GOLPH3 (red). *n*=20 wild-type and *cbe^{z2097/Df}* early telophases; *n*=30 wild-type and *cbe^{z2097/Df}* mid-to-late telophases randomly selected from images taken in five experiments. Scale bar: 10 μ m.

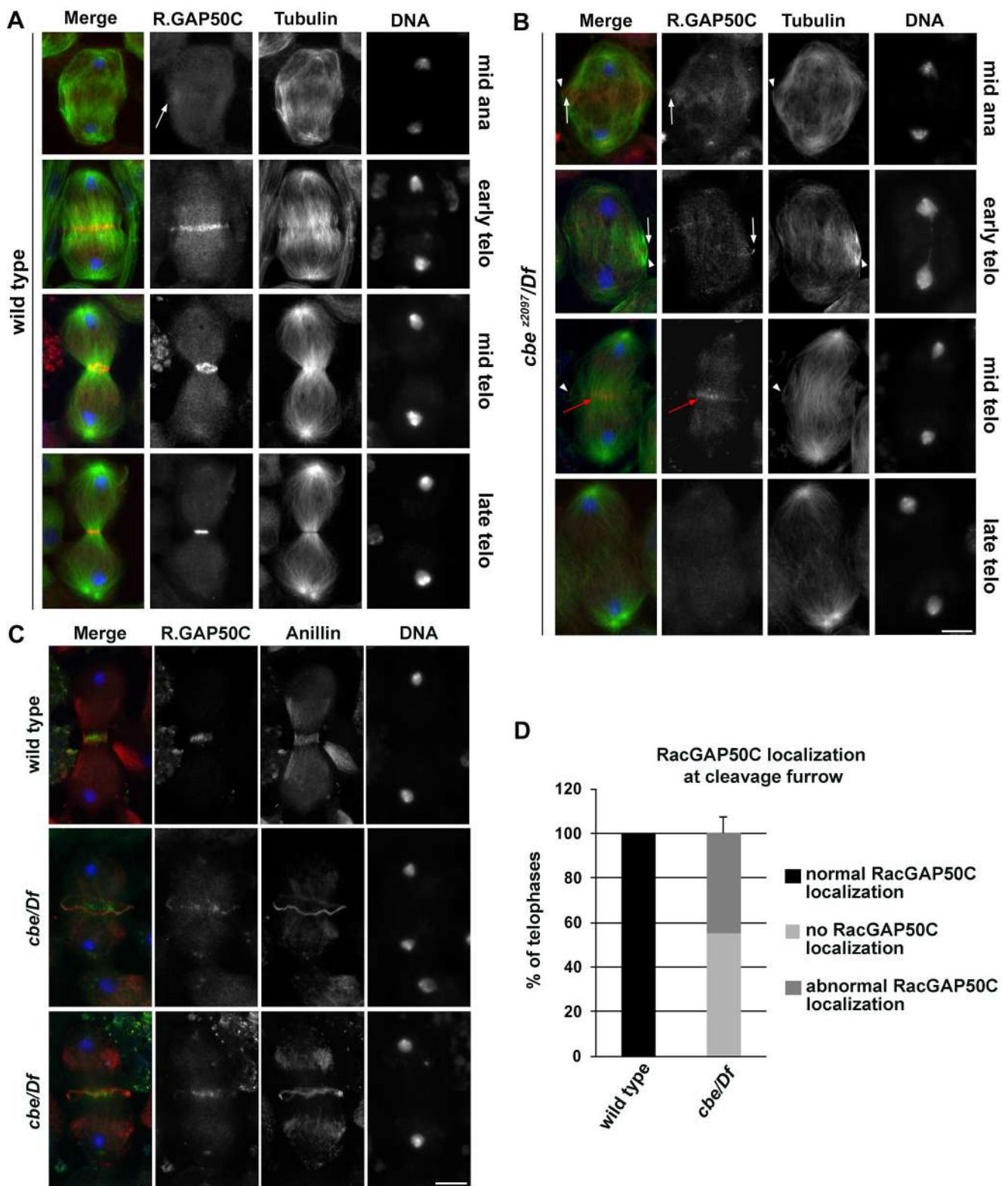


Fig. 5. Localization of RacGAP50C is disrupted in telophase spermatocytes from *cbe^{z2097}* mutant males. (A,B) Wild-type (A) and *cbe^{z2097}/Df(2R)BSC608* (*cbe^{z2097}/Df*) mutant spermatocytes (B) stained for tubulin (green), DNA (blue) and RacGAP50C (R.GAP50C; red). $n=18$ wild-type and *cbe/Df* mid-anaphases; $n=34$ wild-type and *cbe^{z2097}/Df* early telophases; $n=30$ wild-type and *cbe^{z2097}/Df* mid-telophases; $n=50$ wild-type and *cbe^{z2097}/Df* late telophases. Note that in late stages of cytokinesis from *cbe^{z2097}/Df*, RacGAP50C either fails to localize or localizes to interior microtubule bundles of the cell. White arrows point to RacGAP50C accumulation at the peripheral microtubules, arrowheads point to the peripheral microtubules, red arrows point to RacGAP50C at the interior microtubule bundles. (C) Wild-type and *cbe^{z2097}/Df* (*cbe/Df*) mutant spermatocytes stained for RacGAP50C (green), DNA (blue) and Anillin (red). (D) Quantification of defective localization of RacGAP50C in dividing telophase spermatocytes. $n=49$ wild-type and *cbe^{z2097}/Df* telophases, randomly selected from images taken in five experiments. Graph shows mean \pm s.d. percentage. Scale bars: 10 μ m.

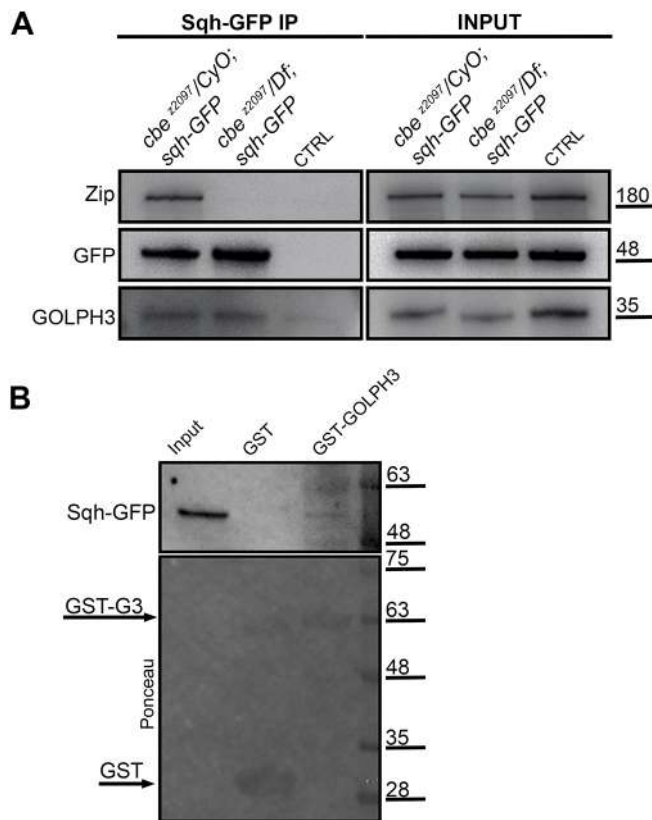


Fig. 6. Co-IP and GST pulldown reveal the interaction of Sqh with Zip and GOLPH3. (A) Protein extracts from testes of the indicated genotypes expressing Sqh-GFP were immunoprecipitated using GFP-binding or control (CTRL) beads and blotted for GFP, Zip and GOLPH3. Testis extracts from Sqh-GFP males were used in control experiments. Input samples (2% of the total lysate) and a third of the immunoprecipitates were loaded and probed with the indicated antibodies. Molecular masses are in kilodaltons. The Co-IP was performed three times with identical results. (B) GST-GOLPH3 (GST-G3) but not GST precipitated Sqh-GFP from testis extracts. Ponceau staining is shown as a loading control. Input (2% of the total extract) and 25% of the pull-down were loaded and probed with the indicated antibodies. Molecular masses are given in kilodaltons.

DISCUSSION

We have shown that *cbe*²⁰⁹⁷, identified during a screen for male sterile mutations affecting spermatocyte cytokinesis, is a missense allele of *Drosophila zipper*. The *cbe*²⁰⁹⁷ allele does not affect female fertility or fly viability in *cbe*²⁰⁹⁷/*Df*, *cbe/zip*¹ and *cbe/zip*² animals. The underlying cause of the different effects of the *cbe* mutation on female and male fertility may depend on sex-specific regulatory mechanisms and different expression patterns of the non-muscle Myosin Zipper isoforms that remain to be clarified. In this context MYH10, the heavy chain of NMIIIB, is required for meiotic cytokinesis in male but not in female mice (Yang et al., 2012).

Although it is widely accepted that actomyosin ring constriction drives cleavage furrow ingression during cytokinesis, the mechanisms that concentrate and stabilize NMII filaments at the equatorial cortex remain poorly understood. Several studies have shown the requirement for the NMHC II Zip for cytokinesis in *Drosophila* cultured cells (Dean et al., 2005; Echard et al., 2004; Eggert et al., 2004; Hickson et al., 2006; Straight et al., 2003, 2005). Analysis of cortical localization of truncated NMHC II proteins in *Drosophila* S2 cells has revealed that preassembled Myosin filaments accumulate at the equatorial cortex in the absence of Rho1 (Uehara et al., 2010). Here, we have shown that *cbe* mutants carry a mutation in a conserved

region of the Zip protein, which replaces an isoleucine residue adjacent to the RLC-binding IQ motif. The hydrophobic amino acid isoleucine is often involved in binding to hydrophobic ligands including lipids. We thus surmise that the replacement of isoleucine with the aromatic amino acid phenylalanine might affect the interaction of NMHC II with the plasma membrane and the assembly of myosin thick filaments at the cleavage site. In agreement with this hypothesis, mammalian NMII proteins have been found to bind to liposomes containing one or more acidic phospholipids but not to liposomes that contain 100% phosphatidylcholine (Liu et al., 2016). Liu et al. (2016) showed that liposome binding of NMIIs to negatively charged liposomes occurs predominantly through the interaction of the liposomes with the RLC-binding site of the heavy chain, suggesting that membrane-bound monomers might associate with regulatory light chains and initiate polymerization of myosin filaments. Remarkably, the short sequence of the NMHC II involved in binding to anionic phospholipids contains a high percentage of hydrophobic amino acids (~55%) and basic amino acids (~24%) (Liu et al., 2016). Similarly, *Acanthamoeba* myosin IC binds to acidic phospholipids *in vitro* through a short sequence of basic and hydrophobic amino acids, named the BH site, located in the non-helical tail (Brzeska et al., 2008). Moreover a BH site in the tail of *Dictyostelium* myosin IB was shown to mediate binding *in vivo* to regions of the plasma membrane enriched with PI(4,5)P₂ and/or phosphatidylinositol (3,4,5)-trisphosphate (Brzeska et al., 2012). Because PI(4,5)P₂ is enriched at the cleavage furrow of dividing spermatocytes (Sechi et al., 2014; Wong et al., 2005), it is likely that wild-type Zip protein might interact with this acidic phospholipid at the furrow plasma membrane.

A recent study showed that the RLC Sqh contributes to PI(4)P localization to the cortical plasma membrane of *Drosophila* neuroblasts, indicating a reciprocal dependence between Myosin II and plasma membrane phosphoinositides (Koe et al., 2018). Our findings demonstrated that *cbe* mutation impairs the association between Zip protein and the RLC Sqh. Despite the lack of Zip-Sqh interaction, *cbe* mutant spermatocytes displayed initial concentration of Zip protein in thin rings at the cleavage site of dividing cells. Recruitment of Sqh was abolished in *cbe* mutants, leading to failure to assemble tight contractile rings and causing cytokinesis failures. These results are consistent with work from Beach and Egelhoff showing recruitment of mammalian NMHC II to the furrow independently of RLC (Beach and Egelhoff, 2009). Overall these data indicate that the mechanisms that concentrate NMHC II at the cleavage site do not require centralspindlin-mediated RLC phosphorylation. However, Zip-Sqh interaction is required for formation of robust actomyosin rings and contractile ring constriction.

Our immunofluorescence analysis of *cbe* mutant dividing spermatocytes showed that Zip protein concentrated in large cytoplasmic aggregates. Zip aggregates have also been reported in embryos and egg chambers from which *sqh* was removed and might result from anomalous heavy chain interactions due to the exposure of the hydrophobic IQ motifs in the absence of binding to regulatory light chains (Edwards and Kiehart, 1996; Franke et al., 2006; Jordan and Karess, 1997; Wheatley et al., 1995). Remarkably, RLC-deficient myosins have been shown to aggregate (Trybus et al., 1994).

In agreement with previous work in *Drosophila* cultured cells by Straight et al. (2005), localization of Anillin at the cleavage furrow did not require NMII filaments, as indicated by normal accumulation of Anillin in early telophase spermatocytes and neuroblasts of *cbe* mutants.

One important conclusion from our study is the reciprocal dependence of GOLPH3 and NMII during the early events of

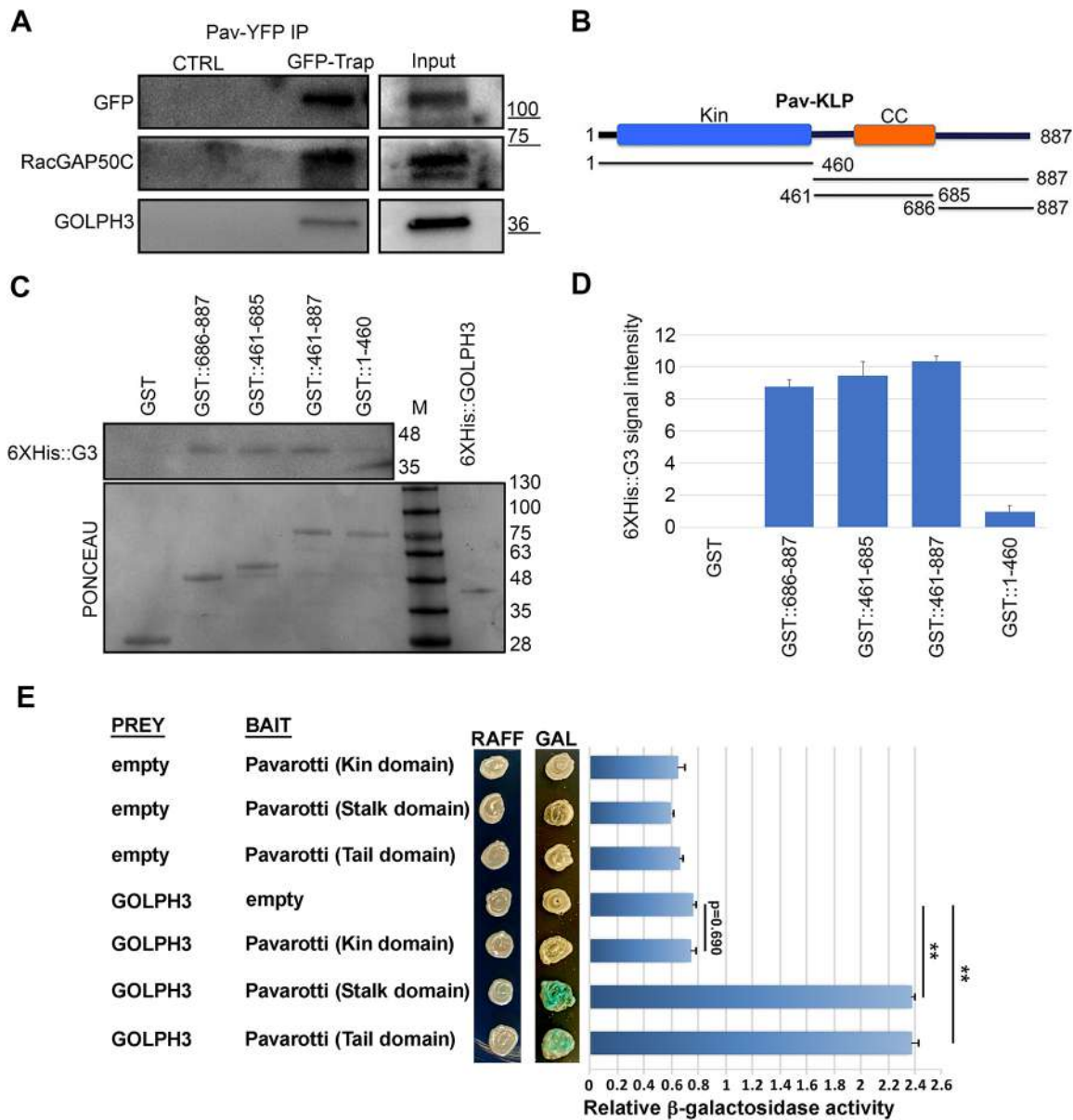


Fig. 7. GOLPH3 binds to Pav protein. (A) RacGAP50C and GOLPH3 co-precipitate with Pav-YFP. Protein extract from testes expressing Pav-YFP was split in half and immunoprecipitated with either GFP-binding (GFP-Trap) or control beads (CTRL) and blotted for YFP, RacGAP50C and GOLPH3. Input sample (2% of the total lysate) and a third of the immunoprecipitates were loaded and probed with the indicated antibodies. The co-IP was performed three times with identical results. (B) Schematic of Pav domains. Amino acids 1–460, motor domain (kin); amino acids 461–685, coiled-coil domain (CC, stalk); amino acids 686–887, C-terminal domain (tail). (C) The three domains of Pav, and the combination stalk plus tail (amino acids 461–887) were expressed as GST-tagged proteins and tested for binding to 6XHis-GOLPH3 (6XHis::G3). Recombinant GST-Pav proteins, immobilized on glutathione beads, were incubated with recombinant 6XHis-tagged GOLPH3. The amount of 6XHis-tagged GOLPH3 that directly bound to each GST-Pav protein or to GST was detected using anti-6XHis antibodies. Ponceau staining is shown as a loading control. 0.1% of the input and 25% of the pulldown samples were loaded and probed with anti-6XHis antibodies. Molecular masses are in kilodaltons. (D) Graph represents quantification of 6XHis-tagged GOLPH3 bound to each form of Pav, as determined by western blot. Protein band intensities were obtained from three independent experiments. Data are mean \pm s.d. (E) Yeast two-hybrid assay to test GOLPH3 interaction with Pav domains. Only the stalk and tail domains induce *lacZ* expression (blue color indicates positive interaction). Quantification of *lacZ* reporter expression (graph) with different combinations of bait and prey plasmids is shown. See Materials and Methods for further details. Mean \pm s.e.m. ** $P < 0.01$ (Mann-Whitney *U*-test). RAFF, raffinose; GAL, galactose.

cytokinesis. Our previous work demonstrated that GOLPH3 function during cytokinesis is intimately connected to its ability to bind to PI(4)P. GOLPH3 recruitment to the cleavage site depends on PI(4)P. Reciprocally, concentration of PI(4)P at the cleavage furrow requires wild-type function of GOLPH3 (Sechi et al., 2014). Moreover, we demonstrated that GOLPH3 function is required to maintain centralspindlin at cell equator and to stabilize Myosin II and Septin rings at the cleavage furrow (Sechi et al., 2014). Based on our findings

in this paper, we propose a model whereby the coordinated function of NMII with GOLPH3 regulates centralspindlin stabilization at the cleavage furrow and contractile ring assembly. As depicted in Fig. 8, initial recruitment of Zip protein at the cleavage site does not require prior binding to Sqh. Robust actomyosin ring formation requires binding to Sqh protein, which enables plasma membrane localization of GOLPH3, and presumably of PI(4)P, at the cleavage site. Consistent with this model, Sqh protein has been shown to bind to

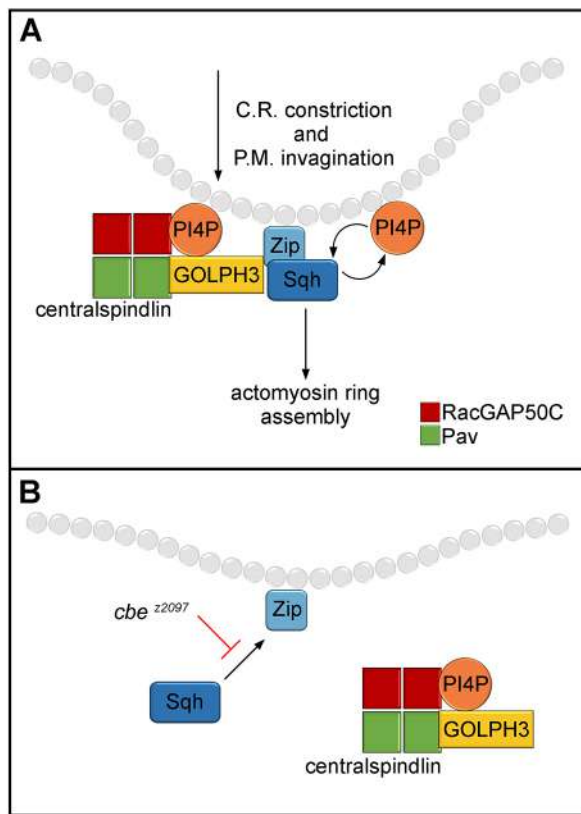


Fig. 8. Diagram depicting the reciprocal dependence of Myosin and PI(4)P-GOLPH3 during early stages of cytokinesis. (A) In dividing wild-type cells, binding of Zip protein to Sqh is required for robust actomyosin ring assembly at the cleavage site. The Zip-Sqh complex interacts with GOLPH3 protein and enables localization of GOLPH3, and presumably of PI(4)P, at the cleavage site. In turn, GOLPH3 controls centralspindlin maintenance at the invaginating plasma membrane by binding to the C-terminal domains of the Pav subunit. Centralspindlin localization at furrow plasma membrane is also stabilized by the interaction of RacGAP50C with polyanionic phosphoinositide lipids, including PI(4)P. (B) In *cbe* mutants, Zip is unable to bind Sqh protein. As a consequence, GOLPH3 fails to accumulate at the cleavage site, resulting in failure to maintain centralspindlin at the invaginating plasma membrane and to undergo cleavage furrow ingression.

PI(4)P *in vitro*, which contributes to its membrane localization in neuroblasts (Koe et al., 2018). Our findings that *Drosophila* GOLPH3 binds to C-terminal domains of Pav suggest that GOLPH3 might regulate the association of centralspindlin with the plasma membrane during cytokinesis and stability of this complex at the invaginating membrane. Centralspindlin localization at the cleavage furrow is likely to also be stabilized by the interaction of RacGAP50C with PI(4)P and other polyanionic phosphoinositide lipids. In agreement with this model, Lekontsev et al. (2012) reported that human CYK4 interacts with PI(4)P and PI(4,5)P₂ phosphoinositides at the furrow plasma membrane via its C1 domain. Moreover, data from Basant et al. (2015) in *Caenorhabditis elegans* showed that the C1 domain of CYK-4 enables association of centralspindlin complex oligomers with the plasma membrane to activate RhoA. In conclusion, our study suggests that a close relationship between NMII filaments and PI(4)P-GOLPH3 may underlie centralspindlin stabilization and contractile ring constriction at the cleavage site. Because Anillin binds to Myosin and RacGAP50C (D'Avino et al., 2008; Gregory et al., 2008; Straight et al., 2005), it is possible that the Anillin-Zipper-Sqh-GOLPH3 module might function as a physical linker between the cleavage furrow and the central spindle during cytokinesis. Indeed, we observed

that the spindle-associated RacGAP50C band loses its association with the Anillin cortical ring in *cbe/Df* telophase spermatocytes. Because GOLPH3, Myosin II and Anillin have all been implicated in tumor formation and progression (Naydenov et al., 2020; Scott et al., 2009; Sechi et al., 2020; Wang et al., 2018), a minute dissection of their roles in the early events of cytokinesis may aid to identify new strategies to treat cancers.

MATERIALS AND METHODS

Fly stocks

Flies were reared according to standard procedures at 25°C. Oregon-R flies were used as wild-type controls unless otherwise specified. The *cbe*^{z2097} mutant strain was identified during a cytological screen of the Zuker's collection of male sterile mutants (Giansanti et al., 2004; Koundakjian et al., 2004). Flies expressing Pav-YFP were provided by M. T. Fuller (Stanford University School of Medicine, Stanford, CA; Szafer-Glusman et al., 2008). The chromosomal deficiencies *Df(2R)BSC604* and *Df(2R)BSC608*, the two alleles *zip*¹ (Zhao et al., 1988) and *zip*² (Young et al., 1993) and P(sqh-GFP.RLC) (Royou et al., 2002) were obtained from the Bloomington *Drosophila* Stock Center (Indiana University, Bloomington, IN).

Microscopy and histology

To quantify multinucleate spermatids, squashed live spermatid preparations were imaged on a Nikon Axioplan epifluorescence microscope equipped with a 40× phase-contrast objective. Cytological preparations for immunofluorescence analysis were made with brains and testes from third instar larvae. To visualize Sqh-GFP with Zip, or GOLPH3 with tubulin, larval testes were dissected in phosphate-buffered saline (PBS), transferred to 5 μl of 4% methanol-free formaldehyde (Polysciences, Warrington, PA, USA) in PBS on a 20×20 coverslip (7 min) and gently squashed. Preparations were then immersed into liquid nitrogen and after coverslip removal with a razor blade, rinsed in PBS (2×5 min). For all other immunofluorescence experiments, preparations were fixed using 3.7% formaldehyde in PBS and then squashed in 60% acetic acid, as previously described in Szafer-Glusman et al. (2011). All samples were permeabilized and blocked in PBS (2×5 min) with 0.1% Triton X-100 (PBT) and 3% BSA before immunofluorescence. Monoclonal antibodies were used to stain α-Tubulin (1:300; Sigma-Aldrich, T6199) and GFP (1:1000; 3E6, Thermo Fisher Scientific). Polyclonal antibodies were as follows: rabbit anti-Zip (1:500; gift of R. Karess, Paris Diderot University, France; Royou et al., 2002); rabbit anti-Sep1 (1:30; gift of J. Pringle, Stanford University, CA; Fares et al., 1995; Field et al., 1996); rabbit anti-RacGAP50C (1:500; gift of D. M. Glover, University of Cambridge, UK; D'Avino et al., 2006); rabbit anti-Cnn (1:300; gift of T. Megraw, Florida State University, FL; Li et al., 1998); rabbit and mouse anti-Anillin (1:1000; Giansanti et al., 2015; Sechi et al., 2017); and rabbit anti-GOLPH3 (G49139/77; 1:1000; Sechi et al., 2014). Secondary antibodies were: Alexa Fluor 555-conjugated anti-rabbit IgG (1:300; Life Technology) and FITC-conjugated anti-mouse IgG (1:30; Jackson ImmunoResearch). All incubations with primary antibodies (diluted in PBT containing 3% BSA) were performed overnight at 4°C. Incubations with secondary antibodies were performed at room temperature for 1 h. After immunostaining, samples were rinsed in PBS and mounted in Vectashield mounting medium with DAPI (H-1800, Vector Laboratories). To stain F-actin with Rhodamine-Phalloidin (Invitrogen), larval testes were fixed in 4% methanol-free formaldehyde (Polysciences, Warrington, PA, USA) in PBS as previously described (Frappaolo et al., 2017a). Images of testes stained for Sqh-GFP and Zip, were taken by an Axio Imager Z1 microscope (Carl Zeiss) equipped with an AxioCam HR cooled charge-coupled camera (Carl Zeiss). All the other images were captured with a charged-coupled device (CCD) camera, Qimaging QICAM Mono Fast 1394 Cooled, connected to a Nikon Axioplan epifluorescence microscope equipped with an HBO 100-W mercury lamp and 40X and 100X objectives.

Molecular cloning

To identify the mutation in the EMS-induced *cbe*^{z2097} allele, the genomic DNA corresponding to *zip* was amplified by PCR and sequenced on both strands (BMR research service). DNA sequences from *cbe*^{z2097}

individuals were compared to sequences of the original Zuker-background chromosome to confirm the point mutation. The pET Directional TOPO Expression kit (Thermo Fisher Scientific) was used to obtain 6×His-GOLPH3 (Sechi et al., 2017).

Co-immunoprecipitation

Co-IP experiments were performed from testes expressing either Sqh-GFP (Fig. 6) or Pav-YFP (Fig. 7) using the procedure described previously (Belloni et al., 2012). For each genotype, 200 adult testes expressing Sqh-GFP were homogenized in 500 µl of lysis buffer [10 mM Tris-HCl pH 7.5, 150 mM NaCl, 0.5 mM EDTA, 0.5% NP40, 1 mM PMSF, 1× protease inhibitor cocktail (Sigma-Aldrich)] for 40 min on ice using a Dounce homogenizer. Lysates were clarified by centrifugation, and protein concentration was quantified using a NanoDrop 2000c Spectrophotometer (Thermo Scientific). For each lysate, 2% was retained as the 'input', the remainder was precleared with control agarose beads (Chromotek, Bab-20). Co-IP was performed using the GFP trap-A or control binding beads purchased from ChromoTek (Planegg-Martinsried), following the protocol that was previously described (Belloni et al., 2012).

Western blotting

Immunoblotting analysis of Zip protein was performed from protein extracts of either adult testes or larval brains. 40 testes or 20 brains from males of each genotype, were homogenized on ice in 100 µl of lysis buffer (10 mM Tris-HCl pH 7.5, 150 mM NaCl, 0.5 mM EDTA, 0.5% NP-40 and 1× protease inhibitor cocktail) using a Dounce homogenizer. Cell lysates were cleared by centrifugation, and protein concentration of supernatants was determined using the Qubit 4 Fluorometer (Invitrogen). Equal amounts of protein were analyzed by SDS-PAGE and western blotting. Samples were separated on Bolt Mini Gels (Novex) and blotted to PVDF membranes (Bio-Rad). Membranes were blocked in Tris-buffered saline (Sigma-Aldrich) with 0.05% Tween-20 (TBS-T; 20 mM Tris-HCl pH 7.5, 150 mM NaCl, 0.05% Tween 20) containing 5% nonfat dry milk (Bio-Rad; Blotting GradeBlocker) for 1 h at room temperature followed by incubation with primary and secondary antibodies diluted in TBS-T. Primary antibodies used for immunoblotting were as follows: mouse anti-GOLPH3 S11047/1/56 (1:2500; Sechi et al., 2014), rabbit anti-GFP (1:1000; TP401, Torrey Pines), rabbit anti-Zip (1:2000; gift from R. Karess), rabbit anti-RacGAP50C (1:500; gift of D. M. Glover; D'Avino et al., 2006); mouse α-Tubulin (1:300; Sigma-Aldrich, T6199), mouse anti-6×His (1:100; Invitrogen, MA1-21315-HRP). HRP-conjugated secondary antibodies were as follows: goat anti-mouse IgG (H+L) (Pierce, N.31431) and goat anti-rabbit IgG (H+L) (Pierce, N.31466). Secondary antibodies were used at 1:5000. After incubation with the antibodies, blots were washed (3×5 min) in TBS-T. Blots were imaged using ECL (Cyanagen, XLS100), and signals revealed with the ChemiDoc XRS imager (Bio-Rad).

Protein expression and GST pulldown

The constructs expressing GST-Pav proteins were a kind gift from P. P. D'Avino (University of Cambridge, UK; Bassi et al., 2013). GST, GST-GOLPH3 and the GST-Pav proteins (GST-Pav¹⁻⁴⁶⁰, GST-Pav⁴⁶¹⁻⁶⁸⁵, GST-Pav⁴⁶¹⁻⁸⁸⁷ and GST-Pav⁶⁸⁶⁻⁸⁸⁷), were expressed in bacteria and purified using glutathione-Sepharose 4B beads (GE Healthcare) following the manufacturer's instructions, as described in Giansanti et al., 2015 and Sechi et al., 2017. 6×His-GOLPH3 was expressed in bacteria and purified using cOmplete His-Tag Purification Resin (Roche). Direct interaction between 6×His-GOLPH3 and GST-Pav proteins was carried out using a protocol described previously (Sechi et al., 2017). The GST pulldown experiment in Fig. 6 was performed with testis lysates using the procedure described in Frappaolo et al. (2017b). At least 200 adult testes were homogenized for 40 min on ice in 500 µl of lysis buffer (25 mM Tris-HCl pH 7.4, 150 mM NaCl, 0.5% NP-40 and 1 mM EDTA) with the addition of protease and phosphatase inhibitor cocktails (Roche), using a Dounce homogenizer. GST pulldown was performed by incubating testis lysates with either GST or GST-GOLPH3 (at the appropriate concentration) bound to glutathione-Sepharose 4B beads (GE healthcare Life sciences), with gentle rotation, at 4°C for two hours. After rinsing in 'wash buffer' (25 mM Tris-HCl pH 7.4, 150 mM NaCl, 1% NP-40, 1 mM EDTA,

protease and phosphatase inhibitors) three times, the beads were boiled in SDS sample buffer, and separated by SDS-PAGE. The bound proteins were analyzed by western blotting. Before immunoblotting, PVDF membranes were stained with Ponceau (Sigma-Aldrich).

Yeast two-hybrid assay

The assay was performed as previously described (Frappaolo et al., 2017b) using the B42/lexA system with strain EGY48 (Mata his3 ura3 trp1 6lexAOP-LEU2; lexAOP-lacZ reporter on plasmid pSH18-34) as the host strain (Cassani et al., 2013). The host strain was co-transformed with various combinations of bait (pEG202) and prey (pJG4-5) plasmids carrying Pav fragments and GOLPH3, respectively. To assess two-hybrid interaction, the strains were spotted on 5-bromo-4-chloro-3-indolyl-β-d-galactopyranoside (X-GAL) selective synthetic plates containing either raffinose (RAFF, prey not induced) or 2% galactose (GAL, prey expressed), as described by Cassani et al. (2013). To quantify the yeast two-hybrid results, a β-galactosidase assay was performed. Strains were first grown in a selective medium containing galactose, then cells were collected, and protein extracts prepared in order to test β-galactosidase enzyme activity using o-nitrophenyl-β-d-galactoside (ONPG) as a substrate, as described by Polevoy et al. (2009). For each sample, five independent transformants were used, and the assays were performed in duplicate to calculate average β-galactosidase units and standard error.

Statistical analysis

For all the immunofluorescence, differences between wild-type and mutant cells were examined for statistical significance using Fisher's exact test with Prism 8 (Graphpad). Quantification of the density of western blot bands used ImageJ (open source image processing program; NIH, Bethesda, MD). Data are expressed as fold changes compared to control. All data represent the mean±s.d. from three independent experiments. Unpaired Student's *t*-test analysis was performed with Prism 8: **P*<0.05; ***P*<0.01; ****P*<0.0001; ns, not significant. For yeast two-hybrid experiments, differences between each group were examined for statistical significance using the Mann-Whitney *U*-test using Prism 8 (Graphpad). *P*<0.05 was considered statistically significant.

Acknowledgements

We thank the Bloomington *Drosophila* Stock Center and M. T. Fuller for fly stocks; D. M. Glover, R. Karess, T. Megraw and J. Pringle for antibodies, P. P. D'Avino for plasmids expressing GST-Pav proteins. We thank A. Berducci for her assistance in the early stages of this work.

Competing interests

The authors declare no competing or financial interests.

Author contributions

Conceptualization: S.S., A.F., R.F., M.G.G.; Methodology: S.S., A.F., R.F., M.G.G.; Validation: S.S., A.F., R.F., M.G.G.; Formal analysis: A.F., A.K.-G., R.F., M.G.G.; Investigation: S.S., A.F., A.K.-G., R.F., M.G.G.; Writing - original draft: M.G.G.; Writing - review & editing: M.G.G.; Visualization: S.S., A.F., A.K.-G., R.F., M.G.G.; Supervision: M.G.G.; Funding acquisition: M.G.G.

Funding

This work was supported by a grant from the AIRC - Fondazione AIRC per la Ricerca sul Cancro (AIRC; grant number IG2017 Id.20779) to M.G.G. A.F. was supported by a fellowship from the Fondazione Italiana per la Ricerca sul Cancro - AIRC (19686).

Supplementary information

Supplementary information available online at <https://jcs.biologists.org/lookup/doi/10.1242/jcs.252965.supplemental>

Peer review history

The peer review history is available online at <https://jcs.biologists.org/lookup/doi/10.1242/jcs.252965.reviewer-comments.pdf>

References

Adams, R. R., Tavares, A. A. M., Salzberg, A., Bellen, H. J. and Glover, D. M. (1998). Pavarotti encodes a kinesin-like protein required to organize the central spindle and contractile ring for cytokinesis. *Genes Dev.* **12**, 1483-1494. doi:10.1101/gad.12.10.1483

- Basant, A., Lekontsev, S., Tse, Y. C., Zhang, D., Longhini, K. M., Petronczki, M. and Glotzer, M.** (2015). Aurora B kinase promotes cytokinesis by inducing centralspindlin oligomers that associate with the plasma membrane. *Dev. Cell* **33**, 204-215. doi:10.1016/j.devcel.2015.03.015
- Bassi, Z. I., Audusseau, M., Riparbelli, M. G., Callaini, G. and D'Avino, P. P.** (2013). Citron kinase controls a molecular network required for midbody formation in cytokinesis. *Proc. Natl. Acad. Sci. USA* **110**, 9782-9787. doi:10.1073/pnas.1301328110
- Beach, J. R. and Egelhoff, T. T.** (2009). Myosin II Recruitment during cytokinesis independent of centralspindlin-mediated phosphorylation. *J. Biol. Chem.* **284**, 27377-27383. doi:10.1074/jbc.M109.028316
- Belloni, G., Sechi, S., Riparbelli, M. G., Fuller, M. T., Callaini, G. and Giansanti, M. G.** (2012). Mutations in Cog7 affect Golgi structure, meiotic cytokinesis and sperm development during *Drosophila* spermatogenesis. *J. Cell Sci.* **125**, 5441-5452. doi:10.1242/jcs.108878
- Brzeska, H., Hwang, K.-J. and Korn, E. D.** (2008). *Acanthamoeba* Myosin IC colocalizes with phosphatidylinositol 4,5-bisphosphate at the plasma membrane due to the High concentration of negative charge. *J. Biol. Chem.* **283**, 32014-32023. doi:10.1074/jbc.M804828200
- Brzeska, H., Guag, J., Preston, G. M., Titus, M. A. and Korn, E. D.** (2012). Molecular basis of dynamic relocalization of Dictyostelium Myosin IB. *J. Biol. Chem.* **287**, 14923-14936. doi:10.1074/jbc.M111.318667
- Cassani, C., Raspelli, E., Santo, N., Chiroli, E., Lucchini, G. and Fraschini, R.** (2013). Saccharomyces cerevisiae Dma proteins participate in cytokinesis by controlling two different pathways. *Cell Cycle* **12**, 2794-2808. doi:10.4161/cc.25869
- D'Avino, P. P.** (2009). How to scaffold the contractile ring for a safe cytokinesis - lessons from Anillin-related proteins. *J. Cell Sci.* **122**, 1071-1079. doi:10.1242/jcs.034785
- D'Avino, P. P., Savoian, M. S., Capalbo, L. and Glover, D. M.** (2006). RacGAP50C is sufficient to signal cleavage furrow formation during cytokinesis. *J. Cell. Sci.* **119**, 4402-4408. doi:10.1242/jcs.03210
- D'Avino, P. P., Takeda, T., Capalbo, L., Zhang, W., Lilley, K. S., Laue, E. D. and Glover, D. M.** (2008). Interaction between Anillin and RacGAP50C connects the actomyosin contractile ring with spindle microtubules at the cell division site. *J. Cell Sci.* **121**, 1151-1158. doi:10.1242/jcs.026716
- D'Avino, P. P., Giansanti, M. G. and Petronczki, M.** (2015). Cytokinesis in animal cells. *Cold Spring Harb. Perspect. Biol.* **7**, a015834. doi:10.1101/cshperspect.a015834
- De Lozanne, A. and Spudich, J. A.** (1987). Disruption of the dictyostelium Myosin heavy chain gene by homologous recombination. *Science* **236**, 1086-1091. doi:10.1126/science.3576222
- Dean, S. O., Rogers, S. L., Turzman, N., Vale, R. D. and Spudich, J. A.** (2005). Distinct pathways control recruitment and maintenance of Myosin II at the cleavage furrow during cytokinesis. *Proc. Natl. Acad. Sci. USA* **102**, 13473-13478. doi:10.1073/pnas.0506810102
- Echard, A., Hickson, G. R., Foley, E. and O'Farrell, P. H.** (2004). Terminal cytokinesis events uncovered after an RNAi screen. *Curr. Biol.* **14**, 1685-1693. doi:10.1016/j.cub.2004.08.063
- Eda, M., Yonemura, S., Kato, T., Watanabe, N., Ishizaki, T., Madaule, P. and Narumiya, S.** (2001). Rho-dependent transfer of citron-kinase to the cleavage furrow of dividing cells. *J. Cell Sci.* **114**, 3273-3284.
- Edwards, K. A. and Kiehart, D. P.** (1996). *Drosophila* nonmuscle Myosin II has multiple essential roles in imaginal disc and egg chamber morphogenesis. *Development* **122**, 1499-1511.
- Eggert, U. S., Kiger, A. A., Richter, C., Perlman, Z. E., Perrimon, N., Mitchison, T. J. and Field, C. M.** (2004). Parallel chemical genetic and genome-wide RNAi screens identify cytokinesis inhibitors and targets. *PLoS Biol.* **2**, e379. doi:10.1371/journal.pbio.0020379
- Fares, H., Peifer, M. and Pringle, J. R.** (1995). Localization and possible functions of *Drosophila* septins. *Mol. Biol. Cell* **6**, 1843-1859. doi:10.1091/mbc.6.12.1843
- Field, C. M., al-Awar, O., Rosenblatt, J., Wong, M. L., Alberts, B. and Mitchison, T. J.** (1996). A purified *drosophila* septin complex forms filaments and exhibits GTPase activity. *J. Cell Biol.* **133**, 605-616. doi:10.1083/jcb.133.3.605
- Franke, J. D., Boury, A. L., Gerald, N. J. and Kiehart, D. P.** (2006). Native nonmuscle Myosin II stability and light chain binding in *Drosophila melanogaster*. *Cell. Motil. Cytoskeleton* **63**, 604-622. doi:10.1002/cm.20148
- Frappaolo, A., Sechi, S., Belloni, G., Piergentili, R. and Giansanti, M. G.** (2017a). Visualization of cleavage furrow proteins in fixed dividing spermatocytes. *Methods Cell Biol.* **137**, 85-103. doi:10.1016/bs.mcb.2016.03.035
- Frappaolo, A., Sechi, S., Kumagai, T., Robinson, S., Fraschini, R., Karimpour-Ghahnavieh, A., Belloni, G., Piergentili, R., Tiemeyer, K. H., Tiemeyer, M. et al.** (2017b). COG7 deficiency in *Drosophila* generates multifaceted developmental, behavioral and protein glycosylation phenotypes. *J. Cell Sci.* **130**, 3637-3649. doi:10.1242/jcs.209049
- Giansanti, M. G. and Fuller, M. T.** (2012). What *Drosophila* spermatocytes tell us about the mechanisms underlying cytokinesis. *Cytoskeleton* **69**, 869-881. doi:10.1002/cm.21063
- Giansanti, M. G., Farkas, R. M., Bonaccorsi, S., Lindsley, D. L., Wakimoto, B. T., Fuller, M. T. and Gatti, M.** (2004). Genetic dissection of meiotic cytokinesis in *Drosophila* males. *Mol. Biol. Cell* **15**, 2509-2522. doi:10.1091/mbc.e03-08-0603
- Giansanti, M. G., Vanderleest, T. E., Jewett, C. E., Sechi, S., Frappaolo, A., Fabian, L., Robinett, C. C., Brill, J. A., Loerke, D., Fuller, M. T. et al.** (2015). Exocyst-dependent membrane addition is required for anaphase cell elongation and cytokinesis in *Drosophila*. *PLoS Genet.* **11**, e1005632. doi:10.1371/journal.pgen.1005632
- Goldbach, P., Wong, R., Beise, N., Sarpal, R., Trimble, W. S. and Brill, J. A.** (2010). Stabilization of the actomyosin ring enables spermatocyte cytokinesis in *Drosophila*. *Mol. Biol. Cell* **21**, 1482-1493. doi:10.1091/mbc.e09-08-0714
- Gregory, S. L., Ebrahimi, S., Milverton, J., Jones, W. M., Bejsovec, A. and Saint, R.** (2008). Cell division requires a direct link between microtubule-bound RacGAP and Anillin in the contractile ring. *Curr. Biol.* **18**, 25-29. doi:10.1016/j.cub.2007.11.050
- Hickson, G. R. X., Echard, A. and O'Farrell, P. H.** (2006). Rho-kinase controls cell shape changes during cytokinesis. *Curr. Biol.* **16**, 359-370. doi:10.1016/j.cub.2005.12.043
- Ishizaki, T., Maekawa, M., Fujisawa, K., Okawa, K., Iwamatsu, A., Fujita, A., Watanabe, N., Saito, Y., Kakizuka, A., Morii, N. et al.** (1996). The small GTP-binding protein Rho binds to and activates a 160 kDa Ser/Thr protein kinase homologous to myotonic dystrophy kinase. *EMBO J.* **15**, 1885-1893. doi:10.1002/j.1460-2075.1996.tb00539.x
- Jordan, P. and Kares, R.** (1997). Myosin light chain-activating phosphorylation sites are required for oogenesis in *Drosophila*. *J. Cell Biol.* **139**, 1805-1819. doi:10.1083/jcb.139.7.1805
- Kamijo, K., Ohara, N., Abe, M., Uchimura, T., Hosoya, H., Lee, J.-S. and Miki, T.** (2006). Dissecting the role of rho-mediated signaling in contractile ring formation. *Mol. Biol. Cell* **17**, 43-55. doi:10.1091/mbc.e05-06-0569
- Kechad, A., Jananji, S., Ruella, Y. and Hickson, G. R.** (2012). Anillin acts as a bifunctional linker coordinating midbody ring biogenesis during cytokinesis. *Curr. Biol.* **22**, 197-203. doi:10.1016/j.cub.2011.11.062
- Ketchum, A. S., Stewart, C. T., Stewart, M. and Kiehart, D. P.** (1990). Complete sequence of the *Drosophila* nonmuscle Myosin heavy-chain transcript: conserved sequences in the Myosin tail and differential splicing in the 5' untranslated sequence. *Proc. Natl. Acad. Sci. USA* **87**, 6316-6320. doi:10.1073/pnas.87.16.6316
- Kiehart, D. P., Lutz, M. S., Chan, D., Ketchum, A. S., Laymon, R. A., Nguyen, B. and Goldstein, L. S.** (1989). Identification of the gene for fly non-muscle myosin heavy chain: *Drosophila* Myosin heavy chains are encoded by a gene family. *EMBO J.* **8**, 913-922. doi:10.1002/j.1460-2075.1989.tb03452.x
- Koe, C. T., Tan, Y. S., Lönnfors, M., Hur, S. K., Low, C. S. L., Zhang, Y., Kancharanwong, P., Bankaitis, V. A. and Wang, H.** (2018). Vibrator and PI4KIII α govern neuroblast polarity by anchoring non-muscle Myosin II. *eLife* **7**, e33555. doi:10.7554/eLife.33555
- Koundakjian, E. J., Cowan, D. M., Hardy, R. W. and Becker, A. H.** (2004). The Zuker collection: a resource for the analysis of autosomal gene function in *Drosophila melanogaster*. *Genetics* **167**, 203-206. doi:10.1534/genetics.167.1.203
- Lekontsev, S., Su, K.-C., Pye, V. E., Blight, K., Sundaramoorthy, S., Takaki, T., Collinson, L. M., Cherepanov, P., Divecha, N. and Petronczki, M.** (2012). Centralspindlin links the mitotic spindle to the plasma membrane during cytokinesis. *Nature* **492**, 276-279. doi:10.1038/nature11773
- Li, K., Xu, E. Y., Cecil, J. K., Turner, F. R., Megraw, T. L. and Kaufman, T. C.** (1998). *Drosophila* centrosomin protein is required for male meiosis and assembly of the flagellar axoneme. *J. Cell Biol.* **141**, 455-467. doi:10.1083/jcb.141.2.455
- Liu, J., Fairn, G. D., Ceccarelli, D. F., Sicheri, F. and Wilde, A.** (2012). Cleavage furrow organization requires PIP2-mediated recruitment of anillin. *Curr. Biol.* **22**, 64-69. doi:10.1016/j.cub.2011.11.040
- Liu, X., Shu, S., Billington, N., Williamson, C. D., Yu, S., Brzeska, H., Donaldson, J. G., Sellers, J. R. and Korn, E. D.** (2016). Mammalian non muscle Myosin II binds to anionic phospholipids with concomitant dissociation of the regulatory light chain. *J. Biol. Chem.* **291**, 24828-24837. doi:10.1074/jbc.M116.739185
- Ma, X., Kovács, M., Conti, M. A., Wang, A., Zhang, Y., Sellers, J. R. and Adelstein, R. S.** (2012). Nonmuscle Myosin II exerts tension but does not translocate actin in vertebrate cytokinesis. *Proc. Natl. Acad. Sci. USA* **109**, 4509-4514. doi:10.1073/pnas.1116268109
- Mabuchi, I. and Okuno, M.** (1977). The effect of Myosin antibody on the division of starfish blastomeres. *J. Cell Biol.* **74**, 251-263. doi:10.1083/jcb.74.1.251
- Mansfield, G. S., Al-Shirawi, D. Y., Ketchum, A. S., Newbern, C. E. and Kiehart, D. P.** (1996). Molecular organization and alternative splicing in zipper, the gene that encodes the *Drosophila* non-muscle Myosin II heavy chain. *J. Mol. Biol.* **255**, 98-109. doi:10.1006/jmbi.1996.0009
- Matsumura, F., Yamakita, Y. and Yamashiro, S.** (2011). Myosin light chain kinases and phosphatase in mitosis and cytokinesis. *Arch. Biochem. Biophys.* **510**, 76-82. doi:10.1016/j.abb.2011.03.002
- Murakami, N., Kotula, L. and Hwang, Y.-W.** (2000). Two distinct mechanisms for regulation of non muscle Myosin assembly via the heavy chain: phosphorylation for MIIb and Mts 1 binding for MIIa. *Biochemistry* **39**, 11441-11451. doi:10.1021/bi000347e

- Naydenov, N., Koblinski, J. and Ivanov, A.** (2020). Anillin is an emerging regulator of tumorigenesis, acting as a cortical cytoskeletal scaffold and a nuclear modulator of cancer cell differentiation. *Cell. Mol. Life Sci.* [Epub] doi:10.1007/s00018-020-03605-9
- Nishimura, Y. and Yonemura, S.** (2006). Centralspindlin regulates ECT2 and RhoA accumulation at the equatorial cortex during cytokinesis. *J. Cell Sci.* **119**, 104-114. doi:10.1242/jcs.02737
- Oegema, K., Savoian, M. S., Mitchison, T. J. and Field, C. M.** (2000). Functional analysis of a human homologue of the *Drosophila* actin binding protein anillin suggests a role in cytokinesis. *J. Cell Biol.* **150**, 539-552. doi:10.1083/jcb.150.3.539
- Osório, D. S., Chan, F. Y., Saramago, J., Leite, J., Silva, A. M., Sobral, A. F., Gassmann, R. and Carvalho, A. X.** (2019). Crosslinking activity of non-muscle Myosin II is not sufficient for embryonic cytokinesis in *C. elegans*. *Development* **146**, dev179150. doi:10.1242/dev.179150
- Piekny, A., Werner, M. and Glotzer, M.** (2005). Cytokinesis: welcome to the Rho zone. *Trends Cell Biol.* **15**, 651-658. doi:10.1016/j.tcb.2005.10.006
- Polevoy, G., Wei, H.-C., Wong, R., Szentpetery, Z., Kim, Y. J., Goldbach, P., Steinbach, S. K., Balla, T. and Brill, J. A.** (2009). Dual roles for the *Drosophila* Pl 4-kinase four wheel drive in localizing Rab11 during cytokinesis. *J. Cell Biol.* **187**, 847-858. doi:10.1083/jcb.200908107
- Ronen, D. and Ravid, S.** (2009). Myosin II tailpiece determines its paracrystal structure, filament assembly properties, and cellular localization. *J. Biol. Chem.* **284**, 24948-24957. doi:10.1074/jbc.M109.023754
- Royou, A., Sullivan, W. and Karess, R.** (2002). Cortical recruitment of non muscle Myosin II in early syncytial *Drosophila* embryos: its role in nuclear axial expansion and its regulation by Cdc2 activity. *J. Cell Biol.* **158**, 127-137. doi:10.1083/jcb.200203148
- Scott, K. L., Kabbarah, O., Liang, M. C., Ivanova, E., Anagnostou, V., Wu, J., Dhakal, S., Wu, M., Chen, S., Feinberg, T. et al.** (2009). GOLPH3 modulates mTOR signalling and rapamycin sensitivity in cancer. *Nature* **459**, 1085-1090. doi:10.1038/nature08109
- Sechi, S., Colotti, G., Belloni, G., Mattei, V., Frappaolo, A., Raffa, G. D., Fuller, M. T. and Giansanti, M. G.** (2014). GOLPH3 is essential for contractile ring formation and Rab11 localization to the cleavage site during cytokinesis in *Drosophila melanogaster*. *PLoS Genet.* **10**, e1004305. doi:10.1371/journal.pgen.1004305
- Sechi, S., Frappaolo, A., Fraschini, R., Capalbo, L., Gottardo, M., Belloni, G., Glover, D. M., Wainman, A. and Giansanti, M. G.** (2017). Rab1 interacts with GOLPH3 and controls golgi structure and contractile ring constriction during cytokinesis in *Drosophila melanogaster*. *Open Biol.* **7**, 160257. doi:10.1098/rsob.160257
- Sechi, S., Frappaolo, A., Karimpour-Ghahnavieh, A., Piergentili, R. and Giansanti, M. G.** (2020). Oncogenic roles of GOLPH3 in the Physiopathology of cancer. *Int. J. Mol. Sci.* **21**, 933. doi:10.3390/ijms21030933
- Shutova, M. S. and Svitkina, T. M.** (2018). Mammalian nonmuscle Myosin II comes in three flavors. *Biochem. Biophys. Res. Commun.* **506**, 394-402. doi:10.1016/j.bbrc.2018.03.103
- Somers, W. G. and Saint, R.** (2003). A RhoGEF and Rho family GTPase-activating protein complex links the contractile ring to cortical microtubules at the onset of cytokinesis. *Dev. Cell* **4**, 29-39. doi:10.1016/s1534-5807(02)00402-1
- Straight, A. F., Cheung, A., Limouze, J., Chen, I., Westwood, N. J., Sellers, J. R. and Mitchison, T. J.** (2003). Dissecting temporal and spatial control of cytokinesis with a Myosin II inhibitor. *Science* **299**, 1743-1747. doi:10.1126/science.1081412
- Straight, A. F., Field, C. M. and Mitchison, T. J.** (2005). Anillin binds nonmuscle Myosin II and regulates the contractile ring. *Mol. Biol. Cell* **16**, 193-201. doi:10.1091/mbc.e04-08-0758
- Szafer-Glusman, E., Giansanti, M. G., Nishihama, R., Bolival, B., Pringle, J., Gatti, M. and Fuller, M. T.** (2008). A role for very-long-chain fatty acids in furrow ingression during cytokinesis in *Drosophila* spermatocytes. *Curr. Biol.* **18**, 1426-1431. doi:10.1016/j.cub.2008.08.061
- Szafer-Glusman, E., Fuller, M. T. and Giansanti, M. G.** (2011). Role of Survivin in cytokinesis revealed by a separation-of-function allele. *Mol. Biol. Cell* **22**, 3779-3790. doi:10.1091/mbc.E11-06-0569
- Takeda, T., Robinson, I. M., Savoian, M. M., Griffiths, J. R., Whetton, A. D., McMahon, H. T. and Glover, D. M.** (2013). *Drosophila* F-BAR protein Syndapin contributes to coupling the plasma membrane and contractile ring in cytokinesis. *Open Biol.* **3**, 130081. doi:10.1098/rsob.130081
- Trybus, K. M., Waller, G. S. and Chatman, T. A.** (1994). Coupling of ATPase activity and motility in smooth muscle myosin is mediated by the regulatory light chain. *J. Cell Biol.* **124**, 963-969. doi:10.1083/jcb.124.6.963
- Uehara, R., Goshima, G., Mabuchi, I., Vale, R. D., Spudich, J. A. and Griffis, E. R.** (2010). Determinants of Myosin II cortical localization during cytokinesis. *Curr. Biol.* **20**, 1080-1085. doi:10.1016/j.cub.2010.04.058
- Vale, R. D., Spudich, J. A. and Griffis, E. R.** (2009). Dynamics of Myosin, microtubules, and Kinesin-6 at the cortex during cytokinesis in *Drosophila* S2 cells. *J. Cell Biol.* **186**, 727-738. doi:10.1083/jcb.200902083
- Vicente-Manzanares, M., Ma, X., Adelstein, R. S. and Horwitz, A. R.** (2009). Non-muscle Myosin II takes centre stage in cell adhesion and migration. *Nat. Rev. Mol. Cell Biol.* **10**, 778-790. doi:10.1038/nrm2786
- Wang, Y., Yang, Q., Cheng, Y., Gao, M., Kuang, L. and Wang, C.** (2018). Myosin heavy chain 10 (MYH10) gene silencing reduces cell migration and invasion in the glioma cell lines U251, T98G, and SHG44 by inhibiting the Wnt/ β -catenin pathway. *Med. Sci. Monit.* **24**, 9110-9119. doi:10.12659/MSM.911523
- Wang, K., Wloka, C. and Bi, E.** (2019). Non-muscle Myosin-II is required for the generation of a constriction site for subsequent abscission. *iScience* **13**, 69-81. doi:10.1016/j.isci.2019.02.010
- Wheatley, S., Kulkarni, S. and Karess, R.** (1995). *Drosophila* nonmuscle Myosin II is required for rapid cytoplasmic transport during oogenesis and for axial nuclear migration in early embryos. *Development* **121**, 1937-1946.
- Wong, R., Hadjiyanni, I., Wei, H.-C., Polevoy, G., McBride, R., Sem, K.-P. and Brill, J. A.** (2005). PIP2 hydrolysis and calcium release are required for cytokinesis in *Drosophila* spermatocytes. *Curr. Biol.* **15**, 1401-1406. doi:10.1016/j.cub.2005.06.060
- Yamashiro, S., Totsukawa, G., Yamakita, Y., Sasaki, Y., Madaule, P., Ishizaki, T., Narumiya, S. and Matsumura, F.** (2003). Citron kinase, a Rho-dependent kinase, induces di-phosphorylation of regulatory light chain of Myosin II. *Mol. Biol. Cell* **14**, 1745-1756. doi:10.1091/mbc.e02-07-0427
- Yang, F., Wei, Q., Adelstein, R. S. and Wang, P. J.** (2012). Non-muscle Myosin IIB is essential for cytokinesis during male meiotic cell divisions. *Dev. Biol.* **369**, 356-361. doi:10.1016/j.ydbio.2012.07.011
- Young, P. E., Richman, A. M., Ketchum, A. S. and Kiehart, D. P.** (1993). Morphogenesis in *Drosophila* requires nonmuscle myosin heavy chain function. *Genes Dev.* **7**, 29-41. doi:10.1101/gad.7.1.29
- Yüce, Ö., Piekny, A. and Glotzer, M.** (2005). An ECT2-centralspindlin complex regulates the localization and function of RhoA. *J. Cell Biol.* **170**, 571-582. doi:10.1083/jcb.200501097
- Zhao, W.-m. and Fang, G.** (2005). MgcRacGAP controls the assembly of the contractile ring and the initiation of Cytokinesis. *Proc. Natl. Acad. Sci. USA* **102**, 13158-13163. doi:10.1073/pnas.0504145102
- Zhao, D. B., Côté, S., Jähnig, F., Haller, J. and Jäckle, H.** (1988). Zipper encodes a putative integral membrane protein required for normal axon patterning during *Drosophila* neurogenesis. *EMBO J.* **7**, 1115-1119. doi:10.1002/j.1460-2075.1988.tb02920.x